Vol.7 No.2 April 2024

Journal of Networking and Communication Systems

Received 28 February, Revised 29 March, Accepted 29 April

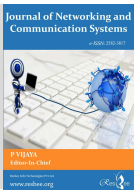

Optimization Driven Deep Convolutional Neural Network and Mean Shift Based Segmentation for Osteoporosis Classification in X-ray Images

Gayathri kommineni

University of Missouri Kansas City, United States
gayathri.kommineni01@gmail.com

Abstract: Osteoporosis occurs due to the fragility fracture of the bone, which mostly affects the women as per the report over 50 years. Various methods are introduced to achieve osteoporosis classification in the X-ray images, but focusing on the cortical bones is a major challenge in the research community. Thus, an Adaptive Gradient Harmony Search (GHS) based Deep Convolutional Neural Network (Deep CNN) is proposed to achieve the osteoporosis classification. Initially, the input images are pre-processed to extract the interesting region and are segmented using the mean shift clustering technique to extract the femur boundaries. The extracted femur boundaries are further processed by the femur bone geometric estimation phase, which uses the template search method to mark the femur points automatically. The features, like medical-level features, image-level features, and pixel-level features are extracted through the feature extraction process. Finally, the osteoporosis classification is achieved using the Deep Convolutional Neural Network, which is trained by the proposed Adaptive Gradient Harmony Search optimization. The implementation of the proposed Adaptive Gradient Harmony Search-based Deep Convolutional Neural Network is carried out and the performance is analyzed using the metrics, namely accuracy, specificity, and sensitivity, which acquire the values of 0.97, 0.99, and 0.99 respectively.

Keywords: Mean Shift, Template Search, Quantitative Imaging, Adaptive Gradient Harmony Search (Adaptive Ghs), Osteoporosis.

1. Introduction

Osteoporosis is one of the harmful bone diseases, that is caused due to the reduction of the bone structure and the bone mass and hence it leads to fragility fracture. Fractures exist in osteoporosis is the main health risk problem, which mostly affects women and less in men at the age of 50. According to the audit report taken in the year 2013 by the Asia Pacific region, osteoporosis affects women in most hospitalizations rather than diabetes through breast cancer or myocardial infarction for above 45 years. However, it is most commonly placed in the elderly population particularly, for postmenopausal women [1]. It is coupled with cortical bone porosity and trabecular bone connectivity, which increases the risk of fracture and bone fragility [7]. The audit report says that in the aging population, the fractures that occur in osteoporosis substantially increase by 2050, when one-third of the population will be aged 50 years especially, in Asia alone 50% of people are affected by global fractures. Osteoporosis is an asymptomatic and painless disease, when fragility fracture arises, the osteoporosis disease may be undiagnosed. Once an initial fracture occurs, then there may be a chance for subsequent fractures, which results in high risk [1] [10]. For women, the range of osteoporotic fracture at high risk is 40% to 50% and in the case of men, it is reported as 13% to 22% [1] [11]. The fragility fracture enhances the mortality and morbidity rate for people, who get affected with osteoporosis [1].

Osteoporosis weakens the trabecular bone structure and diminishes the cortical bones. During osteoporosis onset, the trabecular bone experience changes in the characteristics of bone, and also it offers accurate sensitive measurement to diagnose the disease early [1] [12].Vertebral Fractures (VF) are one of the significance of osteoporosis, which affects nearly 20% of women and 80% of elders above 80 years. VF is incorporated with kyphosis, height loss, functional impairment, back pain, mortality, and an increase in morbidity rate [8] [9]. VF maximizes the hip fracture or the subsequent vertebral fracture from 4 to 12 fold, respectively [8] [20] [21]. Traditional methods, like thresholding, edge and contour-based methods, and spatially discrete utilize the grey level information only, and hence, these are not appropriate for solving the inhomogeneity problems [6]. Such methods require a suitable segmentation scheme to differentiate the objects, while the segmented results can be enhanced using the prior shape

https://doi.org/10.46253/jnacs.v7i2.a5

information [6].In the treatment of osteoporosis, studies, and practices show that this disease can be diagnosed only at the initial fragility fracture otherwise, the bone condition cannot be cured [1] [13]. Hence, it is required for sensitive, accurate, and low-cost methods to diagnose and predict the fracture risk of osteoporosis at an early stage. Even though various biochemical markers, like collagen cross links, osteocalcin, and collagen telopeptide are available in clinical practice, quantitative imaging methods are used in population studies because of their reproducibility and high precision [1] [14] [15]. A quantitative imaging method is introduced to achieve bone density quantification to monitor the therapeutical intervention and diagnose osteoporosis [1].

The most commonly used technique to screen the osteoporosis is Bone Mineral Density (BMD) using Dual Energy X-ray Absorptiometry (DXA) [7]. The genetic swarm fuzzy classifier was introduced in [2]to diagnose the female patients, by partitioning the attributes to determine the rule set and the membership function. Moreover, the optimization and the classification are carried out using the fuzzy inference system. The regression-based SVM is used to diagnose osteoporosis by identifying the significant factors in the regression tree [2] [16]. The k-nearest neighbor classifier uses the X-ray images and the volumetric topological information to diagnose osteoporosis [2] [17]. The support vector machine classifies the osteoporotic data using the fractional motion scheme based on the extracted features [2] [18]. Osteoporosis is predicted using classification algorithms, such as logistic regression, Naive Bayes, and Multilayer Feed-Forward Neural Network (MFFN) [2][19]. It is a skeletal disorder disease, which is due to the loss of BMD. Due to the fragility and the loss of bones, osteoporosis raisesbone fractures without causing any symptoms. The fractures occurring in osteoporosis are more common than breast cancer, strokes, and attacks [3] [22]. Osteoporosis is conclusively diagnosed using the X-ray imaging method named DXA. In the medical sector, DXA is considered as the gold standard in diagnosing the bone diseases. Computed tomography is an alternate method used to analyze the risk of osteoporosis fracture [3] [23].

The primary intention of this work is to design and develop a method for osteoporosis classification. The proposed Adaptive GHS-based Deep CNN classifier achieves osteoporosis classification by involving five phases, namely pre-processing, segmentation, geometric estimation, feature extraction, and classification. At first, the input image is pre-processed in the pre-processing phase to extract the interesting region. The segmentation phase uses the mean shift clustering technique to extract the femur boundaries, which are passed to the femur bone geometric estimation phase, where the femur points are automatically marked based on the template search model. Finally, the osteoporosis classification is carried out using the Deep CNN classifier, which is trained by the proposed Adaptive GHS optimization.

The contribution of this research is elaborated as follows:

- The interesting regions in the X-ray images and the features, like image-level features, medical-level features, and pixel-level features are extracted.
- The femur points in the femur boundaries are automatically marked using the template search method. The proposed Deep CNN classifier is trained using the Adaptive GHS optimization to achieve the osteoporosis classification.

The rest of the paper is organized as the literature survey of the existing methods is elaborated in section 2. The proposed osteoporosis classification approach is elaborated in section 3, and the results along with the analysis are elaborated in section 4. Finally, the conclusion is made in Section 5

2. Motivation

In this section, the motivation of the proposed approach is deliberated, which involves various existing osteoporosis classification methods.

2.1 Literature Survey

Some of the existing methods of osteoporosis bone disease classification along with their merits and demerits are surveyed in this section. Areeckal A.S. and Kocher M [1] modeled a region-growing algorithm to diagnose osteoporosis. It used the edge detection approach to segment the lumbar vertebra and the femur bones. The seed point was automatically or manually placed inside the homogeneous region. The texture analysis and the density measurement of the bones were combined to achieve osteoporosis detection. However, this algorithm offered accurate sensitive measures, but it failed to characterize the bones. Devikanniga D. and Raj R.J.S [2] introduced the monarch butterfly optimization algorithm to prevent and diagnose osteoporosis at an early stage. This algorithm used the Artificial Neural Network (ANN) to achieve the classification of the osteoporotic. This algorithm was suitable and flexible to perform data classification in the medical field for high-dimensional data. However, the problems that existed in the medical domain were not considered. Hussain D. and Han S.M [3] developed

a Computer-aided osteoporosis detection method (CAOD) to measure bone density and to generate the report from the dual energy X-ray scan (DXA). CAOD segmented and denoised the scan images using the mean filter. The pixels were classified as either tissue or bone and then, the contours were extracted effectively. Moreover, this method enhanced the system performance and attained better accuracy, but was not suitable for large-sized data. Aouache M *et al.*[4] modeled a fuzzy decision tree-based approach to perform the osteoporosis classification. It obtained better classification performance and diagnostic system with limited computational complexity. However, classifying the lumbar vertebrae in osteoporosis was not achieved. Gazzotti M.R *et al.*[5] introduced a semi-quantitative approach to perform the osteoporosis diagnosis. The thoracic fractures of the patient were collected based on the osteoporosis frequency to perform the clinical diagnosis. However, it attained better efficiency, but the mineral density of the bone was not measured. Aslan M.S *et al.*[6] introduced a universal shape and probabilistic model to achieve vertebral body segmentation. The probabilistic energy was optimized using the piece of information, like shape, intensity, and spatial interaction. This model was more robust and fast enough under noise levels but was not reliable in providing the clinical software. Kavitha M.S *et al.*[7] modeled a genetic swarm fuzzy classifier to diagnose female patients using the mineral density of the bone. The attributes of the trabecular bone and the mandibular bones were obtained efficiently. It generated the membership function to screen osteoporosis by dividing the geometrical attributes. However, this approach attained better diagnostic performance, but it resulted in poor accuracy. Deleskog L *et al.*[8] modeled a semi-quantitative approach to diagnose spine fractures. It used the DXA scan images to detect the fractures by visualizing the upper spine. It attained better diagnostic performance, but the vertebral fracture detection was poor.In 2023, Hwang *et al.* [32] implemented the DL method for the diagnosis of osteopenia and osteoporosis. Initially, the CT scan was pre-processed through the Hounsfield unit (HU) and fed into the MVCT net to extract its features. The extracted image used images as a separate image input and learned different features through dissimilarity loss. After that, the target layers learned the target task through the features of the two feature extractors and then aggregated them. Finally, the output of the MVCT Net classified bone density as normal, osteopenia, or osteoporosis. The result showed that the proposed method automatically identifies osteoporosis through CT images without manual work. However, this method experimented with a single dataset. In 2023, Zhang *et al.* [33] have executed the DL method for the classification of osteoporosis. This method consists of various modules. Initially, the input images were localized into vertebral bodies. Then the vertebral bodies were segmented into individual vertebrae. The segmented images extracted features from the segmented vertebrae and used a gated convolution module to adjust its context features integrate segmentation and classification features and adjust the weight of different levels of vertebrae. Finally, the output of the model was then classified into normal, osteopenia, or osteoporosis. The output was more accurate than the existing method but the computational cost of the process was higher. In 2023, Alqahtani *et al.* [34] experimented with using semi-automated software to point out the outline of the vertebral body through DXA images. Initially, the images were drawn. Using the AVERT software the process was automated and the images were displayed it the laptop screen. From which the image annotated the center of each vertebral body manually. The software also predicts the points in the vertebral body through RFRV-CLM. Finally, a manual correction was carried out to predict the exert points in the vertebral body. This method used only small sample images and required manual prediction. In 2023, Albuquerque *et al.* [35] have used osseous for screening osteoporosis. Initially, this device measured the attenuation of the signal that crossed the medial phalanx of a patient's middle finger using electromagnetic waves. Then they analyzed the performance of Osseus by predicting changes in bone mineral density using Osseus measurements and identified the common risk factors as input features to a set of supervised classification models. Finally, the results from DXA were taken as target values during the training of the machine learning algorithms. The result suggested RF algorithm provides better results than other algorithms. However, this method was costly. In 2023, Hsu *et al.* [36] applied a two-compartment model (TCM) for the lumbar spine using a CT scan. Initially, CT image from the patients was taken as input to identify the relationship between the linear attenuation coefficient of the X-ray spectrum and the coefficient of water in the linear attenuation. Water was used to equivalent bone marrow. Then using phantom calibration, the output was extracted and the region of interest was calculated. The accuracy was obtained through vBMD and the TCM method was used to calculate the energy dependency. This method helped in the early detection of osteoporosis. This method was only applied to the lumbar spine and not applied to any other parts of the body. In 2023, Al-Bogami *et al.* [37] adopted various tests to identify the responsiveness of the therapy of osteoporosis. Initially, a DXA scan was collected from the patients. Therapy was performed to identify patients. They noted the BMD variation of the patients along with the lumbar spine and hip respectively. This helps to prevent bone loss and is effective for the treatment of osteoporosis. However, this method didn't consider fracture risk or quality of life. In 2022, Wani *et al.* [38] have ensembled DL to detect osteoporosis from knee X-rays. Initially, X-rays from the knee were collected and formed a dataset. The dataset was then split into training and tested data. The training

data was then augmented to increase the number of images in the trained set. Furthermore, training was carried out through the CNN model using transfer learning. Finally, the x-ray image was then evaluated and compared performance into normal, osteopenia, and osteoporosis disease groups. This method helped to detect osteoporosis in the early stage and reduce the risk of fractures. Other X-ray images apart from the knee were not considered. In 2022, Mohammed *et al.* [39] have applied Duel energy X-ray absorptiometry (DEXA) image. Initially, the original images from the dataset were loaded. Then the image was pre-processed to remove external noise and other parts. After that, the image was smoothened to increase the contrast in the required area. Further, Classification was carried out through CNN to extract unique features and to classify the image. Finally, the output of the classified result, indicates whether the image was indicative of osteoporosis or not. The system achieved high accuracy in the classification of images. This method however not applicable to other bone diseases.

2.2 Challenges

The challenges of the research are:

- Diagnosing and predicting the fracture risk of osteoporosis is highly precise. Monitoring the therapeutical interventions in the biochemical marker is a major challenge associated with bone quantification [1].
- Extracting and segmenting the data from the DXA images is a quite challenging task in the osteoporosis diagnosis, as it uses the mean filter for image de-noising [3].
- Due to the osteophytes, inner boundaries, weak edges, and double boundary of the spine bones, segmenting the osteoporosis disease using the computed tomography (CT) image is a major challenge in the femur fracture classification [6].
- Classifying and segmenting the cervical vertebrae of the vertebrae fracture as abnormal or normal at the early stage is a difficult task in the field of medical diagnosis [4].
- Managing and finding the individual with high fracture risk, and the responsibility of the policy makers for providing the health-care to the bone disease is a key challenge in the healthcare professionals [13].

3. Proposed Adaptive GHS-based Deep CNN classifier for osteoporosis classification

Osteoporosis is a harmful disease, which affects the bones and leads to bone fragility by minimizing bone density. The fracture in the bone causes severe backache, height loss, and bone deformities, which significantly affect the vertebrae. Hence, there is a necessity to perform the osteoporosis classification at the early stage using X-ray images. The proposed Adaptive GHS-based Deep CNN classifier performs the osteoporosis classification that involves five phases, namely pre-processing, segmentation, geometric estimation, feature extraction, and classification. The input X-ray image is pre-processed for extracting the interesting region and is passed into the segmentation phase. The segmentation process uses the mean shift clustering technique to extract the femur boundaries. The extracted femur boundaries are subjected to the femur bone geometric estimation phase, which utilizes the template search method to mark the femur points automatically. In the feature extraction phase, the features like medical-level features, image-level features, and pixel-level features are extracted. Finally, the osteoporosis classification is performed using the Deep CNN classifier, which is trained by the proposed Adaptive GHS optimization. Adaptive GHS is obtained by incorporating the Adaptive scheme into the Harmony Search (HS) algorithm. The classification determines whether the patient is affected with osteoporosis or not by labeling the data as osteopenia, normal, and osteoporosis. Fig. 1 illustrates the architecture of the proposed Adaptive GHS-based Deep CNN for osteoporosis classification.

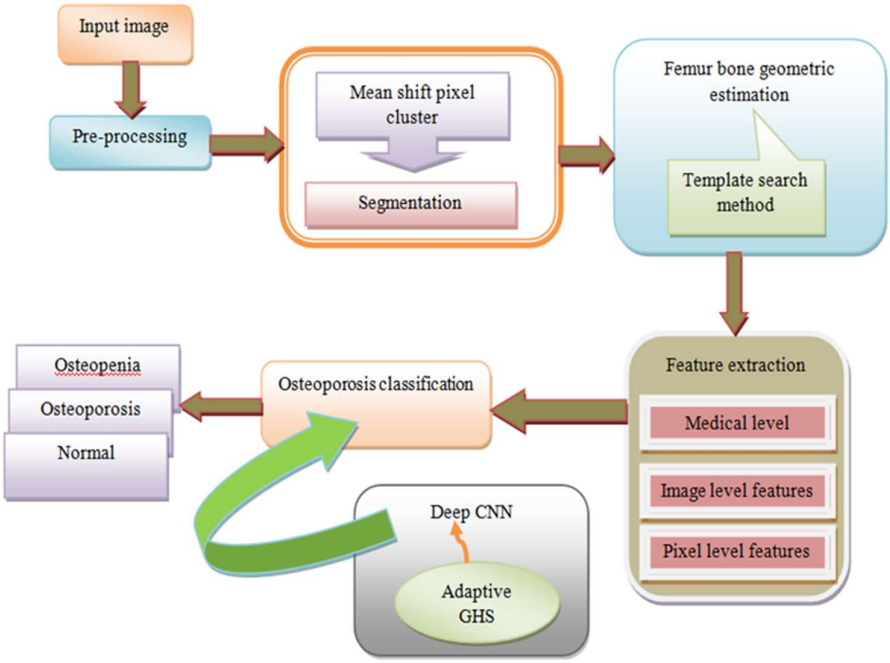

Fig. 1.*The architecture of the proposed Adaptive GHS-based Deep CNN*

3.1 Pre-Processing

The initial step in the optimization and mean shift-based segmentation for osteoporosis classification is pre-processing, which makes the image fit for further processing. It is very essential to perform the pre-processing module. As the quality of the image may be poor, by doing the pre-processing process the resulting images are more suited for further processing. By using the pre-processed image, the performance and the quality of the features can be enhanced. Hence, the pre-processed is the best fit for performing the segmentation and the geometric estimation process.

3.2 Segmentation Using Mean Shift Pixel Cluster

The pre-processed images are processed using the segmentation phase for which the mean shift pixel cluster technique [26] is employed that extracts the femur boundaries. The mean shift pixel cluster is the density estimation scheme used to segment the femur boundaries in the X-ray images. Let us consider a data points as, F_m, $m=1,.....,a$ with the dimensional space as A^e is expressed as

$$g(F)=\frac{1}{n}\sum_{m=1}^{a} M_B(F-F_m) \tag{1}$$

where, $M(F)$ denotes the kernel density estimator, and B represents the bandwidth matrix.

The multivariate kernel is generated using the kernel of symmetric univariate and is expressed as,

$$M^R(F)=\prod_{m=1}^{e} M_1(b_m) \tag{2}$$

where, $M^R(F)$ denotes the multivariate kernel, which is radially symmetric in nature. The radially symmetric kernels must satisfy the following class,

$$M(F)=h_{d,e}d\left(\|F\|^2\right) \tag{3}$$

where, $d(F)$ denotes the kernel profile, which has the value of $F\geq 0$, and $h_{d,e}$ represents the normalization constant, which makes the value of $M(F)$ as strictly positive when it is integrated with other. When the parameterized value increases then, the bandwidth matrix B is selected as the diagonal $B=diagonal\left[c_1^2,.....c_e^2\right]$ or proportional to the matrix $B=c^2C$ .The main advantage of the mean shift cluster technique is that it offers the bandwidth parameter as, $c>0$. The validity of the Euclidean metric used in the feature space is also provided in the identity matrix. The kernel density estimator employed using the bandwidth parameter is expressed as,

$$\hat{g}(F)=\frac{1}{ac^{e}}\sum_{m=1}^{a}M\left(\frac{F-F_{m}}{c}\right) \tag{4}$$

The estimator of the kernel density is computed using the mean square error of the density. Moreover, the asymptotic approximation of the mean square error is also calculated. In the asymptotic notation, the data points are denoted as, $a\to\infty$, and the bandwidth rate is indicated as, $c\to 0$ with the rate of a^{-1}. For multivariate kernel, the asymptotic approximation is represented as,

$$d_{D}(b)=\begin{cases}1-b & 0\le b\le 1\\ 0 & b>1\end{cases} \tag{5}$$

The normal kernel estimator is symmetrically truncated with the asymptotic measure to obtain the kernel to have a finite support. The density estimator for the arbitrary kernels by adopting the profile notation is represented as,

$$\hat{g}_{c,M}(F)=\frac{h_{d,e}}{ac^{e}}\sum_{m=1}^{a}d\left(\left\|\frac{F-F_{m}}{c}\right\|^{2}\right) \tag{6}$$

The initial step used in the feature space analysis is to identify the number of modes situated in the density. Mostly, the modes are placed at the zero gradient as $\nabla g(F)=0$ and the procedure attached to the mean shift is a well-designed way of locating the zeros without defining the density.

3.3 Geometric Estimation Using A Template Search Method

The femur boundaries extracted and segmented through the segmentation process are further processed by the femur bone geometric estimation using the template search approach to mark the femur points automatically. Here, the significant results of the femur bones are accurately highlighted to achieve different medical-level characteristics from the segmented femur using the template search scheme. The significant femur points from the femur boundaries are computed by the template search method, which gains more advantages in computing the accurate femur points than the existing techniques. Estimating the geometrical features of the bone segments is manually performed, but it may cause poor accuracy, as the manual marking has low knowledge regarding the femur boundaries. As the femur structure of the bone varies for each marking, the femur points in the femur boundaries result in poor accuracy. Hence, the template search method is introduced to mark the femur points automatically in the landmark, which adds more benefits to the research area. Thus, the estimation of the femoral points in the boundaries accurately defines the bone strength and the fracture risk. Fig. 2 shows the template search method for femur bone geometric estimation. The steps involved in measuring the geometrical features of the femur are explained as follows:

Step 1: Applying Circular Hough Transform: The circular portion that appears in the segmented femur is detected using the circular hough transform, and the center location is identified in the femur points. The center femur point is called the optimal center and is represented as, G.

Step 2: Locate the points Hand E: A horizontal line is struck through the optimal center with G as center, and in the horizontal line draw the angle with 35 degrees marked. Again, a line is drawn to the femur boundary at H and E using the optimal center, respectively.

Step 3: Mark point L: The line, that that joins the points H and E is considered, and the distance of HE is partitioned as eight to obtain the distance measure of 'b'. The line H is drawn outward to meet the point L, which is the distance measure of 'b' from H.

Step 4: Draw a perpendicular bisector with 'G' as the optimal center: From the line LE, the perpendicular bisector is extended to meet the points C and I with '*G*' as the center. A parallel line is extended to *BJ* based on *CI* and so a horizontal line is drawn, which cuts the femur boundaries by dividing the lines into three points.

Step 5: Locate the point N: A horizontal line is drawn at points *O* and *D* and from the midpoint of line *OD,* a perpendicular line is drawn, which meets line *LE*. The point, which meets the line LE is marked as, N and is called the femur shaft. Hence, these points are calculated using the template search approach, which identifies the femur points in the femur boundaries automatically to ensure the calculation of the femur features at the medical level.

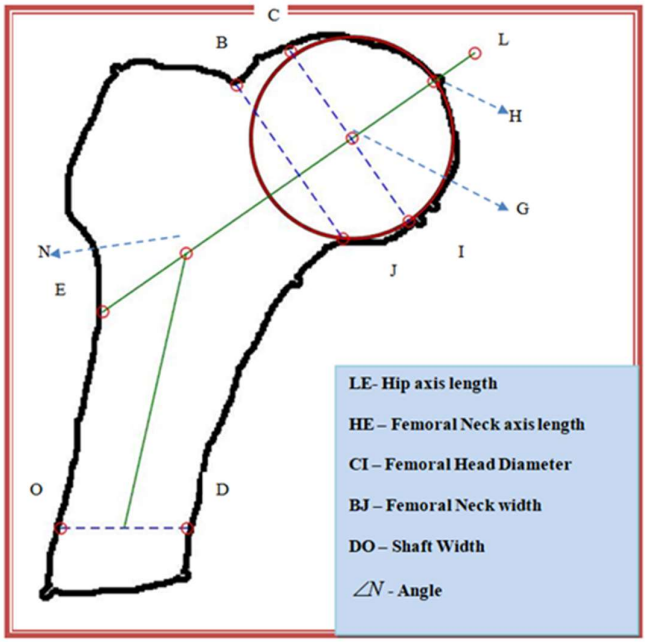

Fig. 2. *Template search method for femur geometric estimation*

3.4 Feature Extraction

The femur points are further processed using the feature extraction phase to extract the features, like medical-level features, image-level features, and pixel-level features. The femur points detected using the template search method are passed into the femur feature extraction stage, where the medical features are extracted from the femur geometrical points. Moreover, the features at the image level are extracted using the pixel coverage information.

3.4.1 Medical Level Features

To achieve effective osteoporosis classification and to increase the classification accuracy, it is required to extract the medical features from the femur points. The medical features collected from the femur segments are, neck shaft angle (NSA), femoral head diameter (FHD), shaft width (w), hip axis length, femoral neck width (FNW), and femoral neck axis length (HAL), which are extracted using the geometrical points of femur determined by the template search method.

*a) FHD:*FHD is defined as the strength of the femur, which is the measure of distance between the femur points *C* and *I* shown in Fig. 2. However, the measure with the maximum value is selected from the diameter of the femoral head.

b) Shaft width: The shaft width is defined as the width of the femur that is situated under the trochanter minor. In Fig. 2, the line *DO* defines the shaft width.

c) NSA: The neck shaft angle is the angle measured between the shaft axis and the femoral neck axis and is indicated as, $\angle N$. The NSA angle is usually found in the range of $120^{\circ} - 135^{\circ}$ for adults, but it changes for the individual depending on the physical activity.

d) HAL: HAL is the distance measured between the inner pelvic brim and the greater trochanter. In Fig. 2, the point *L* denotes the greater trochanter and the point *E* denotes the inner pelvic brim, while *LE* defines the hip axis length. However, longer HAL shows that the bone is at high risk of fracture, but it is the best indicator of bone diseases.

e) FNW: The femoral neck across the neck axis with the narrowest distance is FNW. The distance measure between the points *O* and *E* in Fig. 2 shows the analysis of FNW. It clearly shows that if FNW is low then, the risk associated with the bone is high. Moreover, FNW is incorporated with size, age, and other parameters in the body.

f) FNAL: The distance between the femoral head *E* and the greater trochanter *H* is defined as FNAL. When the femur is affected by the connective tissues, the FNAL is used to keep the femur isolated. Points *E* and *H* in Fig. 2 show the FNAL measure.

3.4.2 Image Level Features

The pixel-wise estimation is used to extract the image level features, like entropy, kurtosis, variance, mean, and skewness. The mean feature is expressed as,

$$\lambda = \frac{1}{a}\sum_{m=1}^{a}\delta_m \tag{7}$$

where λ represents the mean, a denotes the number of pixels present in the X-ray image, and δ_m denotes the m^{th} pixel of the X-ray image. The extraction of the texture features from the femur image is the major advantage of mean determination, as it offers better classification in the femur image. Moreover, the variance of the femur image is represented as,

$$\mu = \frac{1}{a}\sum_{m=1}^{a}\left(\delta_m - \lambda\right) \tag{8}$$

where, μ represent the variance of the femur points. Accordingly, the entropy is computed using the below equation,

$$z(\delta_m) = \sum_{m=1}^{u(\delta_m)} R_m \log R_m \tag{9}$$

where, $u(\delta_m)$ represents the unique femur image pixel points. Based on the entropy value and the pixel intensity, the entropy value of the femur image is computed. When the difference between the neighboring pixel intensity is high then, the entropy value also increases. Kurtosis is defined as the measure of light or heavy-tailed parameter, which depends on the normal distribution and is represented as, M . Skewness is defined as the measure of the asymmetry and is indicated as, H .The image level and the medical level features are combined to obtain the feature vector for the femur image, which is expressed as,

$$V = \left\{v_1, v_2, ,.....v_f, ...v_n\right\} \tag{10}$$

where, n denotes the femur segmented features, which is equal to 11, and so the feature vector dimension of the femur segment is denoted as, $[1\times 11]$. The feature vector of the femur segment, like FHD, NSA, w, HAL, FNW, FNAL, λ , μ , $z(\delta_m)$, H , and M , respectively. Meanwhile, FHD, NSA, w, HAL, FNW, and FNAL are the medical level features and λ , μ , $z(\delta_m)$, H , and M are the image level features.

3.5 Classification based On the Proposed Adaptive GHS-Based Deep CNN for Osteoporosis

The osteoporosis classification is performed using the proposed deep CNN classifier, which is trained by the Adaptive GHS optimization algorithm. The Adaptive GHS is formed by incorporating the Gradient Descent Algorithm with the Harmony Search (HS) [25] algorithm based on the error values.

3.5.1 Architecture of Deep CNN

Deep CNN [24] effectively performs the osteoporosis classification and attains better classification results in the femur points. The architecture of deep CNN has three different layers, a convolutional (conv) layer, a pooling layer, and a fully connected layer. Every layer present in the deep CNN computes unique functions. The convlayer in the deep CNN classifier computes the feature map and is further sub-sampled by the pooling layer. Finally, the classification is performed to identify the fractured bones using the fully connected layer. By introducing more convlayers in the deep CNN classifier, the classification accuracy is enhanced. The neuron of the first layer is connected with the individual neurons at the next layer. Fig. 3 depicts the architecture of the deep CNN classifier.

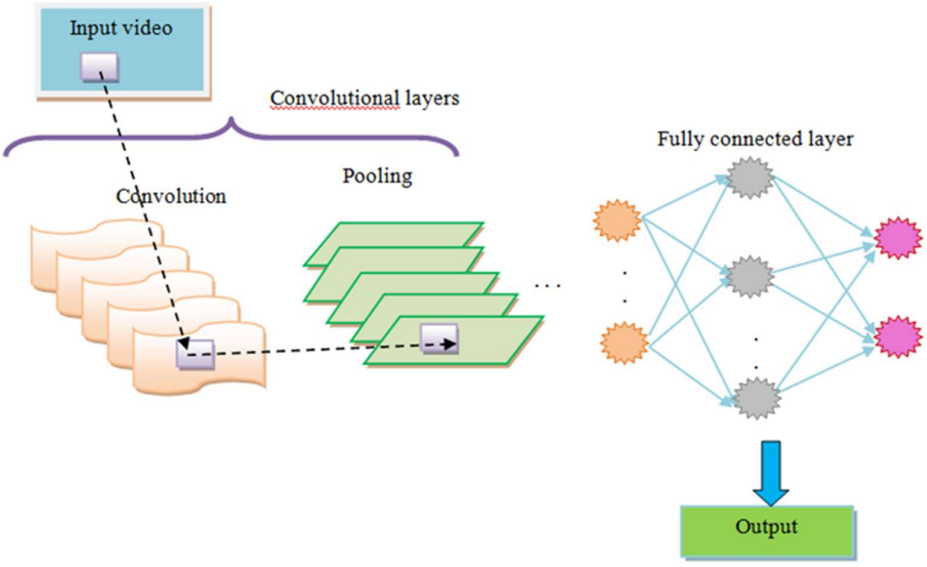

Fig. 3.*The architecture of Deep CNN*

Convolutional layer: The convlayer generates the patterns for the femur points using the convolutional filter, which connects the neurons from the previous layer to the next layer with the help of trainable weights. Let us consider the input of the convlayer as, P and the output of the convlayer is expressed as,

$$\left(P_i^j\right)_{p,q} = \left(S_i^j\right)_{p,q} + \sum_{x=1}^{e_1^{x-1}} \sum_{v=-e_1^j}^{e_1^j} \sum_{y=-e_2^j}^{e_2^j} \left(\omega_{i,x}^j\right)_{y,v} * \left(P_x^{j-1}\right)_{p+v,q+y} \tag{11}$$

where, $\left(P_i^j\right)_{p,q}$ denotes the output of j^{th} convolutional layer or feature map that is present at the center of the femur boundaries, and $*$ denotes the convolutional operator. The output generated from the $(j-1)^{th}$ layer is passed as the input of the next k^{th} convolutional layer. $\omega_{i,x}^j$ represents the weight and S_i^j denotes the bias of j^{th} convolutional layer.

Pooling layer: The pooling layer is otherwise called a non-parametric layer, which performs the fixed operation without the usage of weights and biases.

Fully connected layers: The output generated from the pooling layer is passed as the input of the fully connected layer. The output attained from the fully connected layer is expressed as,

$$T_i^j = \mu\left(P_i^j\right) \tag{12}$$

The weight values are estimated to tune the deep CNN to retrieve the optimal weight.

3.5.2Proposed Adaptive GHS Algorithm For Optimal Tuning Of The Deep CNN Classifier:

HS algorithm is mainly used in the improvisation process to enhance the harmonious state of the musical instrument. Moreover, the harmony of the pitch is estimated as subjective and aesthetic. The solution estimation is performed by placing the decision variable into the fitness function and the function value is evaluated based on factors, like efficiency, error, and cost. The pitch of the musical instrument defines the aesthetic quality and the function value determines the decision variable. The optimization process obtains the global optimum solution by evaluating the objective function. In the musical instrument, the aesthetic quality is computed from the pitch. The HS algorithm is developed from the natural musical performance process, which occurs when the musician searches for the perfect harmony state. Table 1 depicts the pseudo-code of the HS algorithm.

Table 1. *Pseudo code of the proposed GHS algorithm*

Sl. No	GHS meta heuristic algorithm
1	Initializing the algorithm parameters and the optimization problem
2	Initialization of harmony search
3	New harmony generation
4	Memory update for harmony
5	Continue steps three to four until the harmony search condition satisfies

4. Results and Discussion

This section elaborates on the results and discussion of the proposed Adaptive GHS-based deep CNN classifier for osteoporosis classification. The effective result of the proposed approach is attained through the comparative analysis.

4.1 Experimental Setup

The experimentation of the proposed Adaptive GHS-based deep CNN is carried out in the MATLAB tool using the real-time dataset. The MATLAB tool works under the operating system of Windows 8.

4.2 Database Description

The database used in the proposed approach is the real-time database, which is built by collecting real-time information from the persons of the Chennai location. The X-ray images are collected from around 50 persons and the database of the X-ray image is obtained from persons the age of 25 to 81 years to perform the osteoporosis classification. The database used to perform the analysis has 50 men and 50 women. Hence, it is clearly defined that, the patients most affected by the osteoporosis disease are the aged persons.

4.3 Comparative Methods

The performance of the proposed Adaptive GHS-based deep CNN is analyzed and compared with the existing methods, namely Gradient Harmony Search-Deep Belief Network (GHS-DBN), Deep Belief Network (DBN) [27], K-Nearest Neighbor (KNN) [28],Support Vector Machine (SVM) [29], Neural Network, Biogeography-Based Optimization (BBO) [30], and Adaptive Elitist Differential Evolution algorithm (AEDE) [31].

4.4 Experimental Results

This section elaborates on the results of the proposed Adaptive GHS-based deep CNN to the metrics, such as accuracy, specificity, and sensitivity. Fig. 4 depicts the sample results of the osteoporosis classification. Fig. 4 a) depicts the resulting output of mean shift image-1, fig. 4 b) depicts the output of the mean shift image-2, fig. 4 c) depicts the output of the mean shift image-3, and fig. 4 d) depicts the output of mean shift image-4. Fig. 4 e) shows the extracted bone image-1, fig. 4 f) shows the extracted bone image-2, fig. 4 g) depicts the extracted bone image-3, and fig. 4 h) shows the extracted bone image-4, respectively.

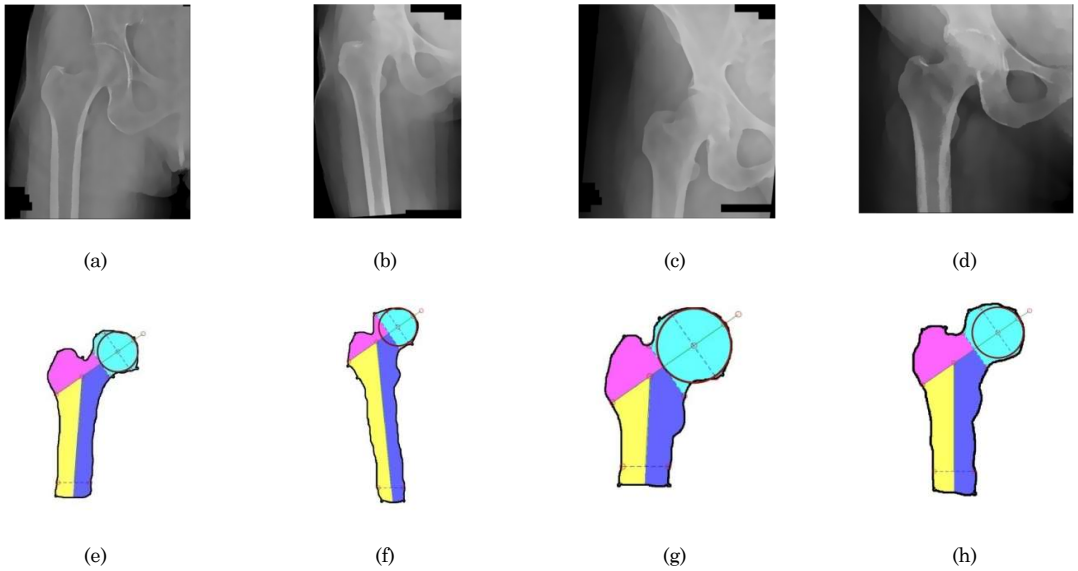

Fig. 4. *Sample results, a) Output of mean shift image-1, b) Output imag eof mean shift image-2, c) Output image of mean shift image-3, d) Output of mean shift image-4, e) Extracted bone image-1, f) Extracted bone image-2, g) Extracted bone image-3, h) Extracted bone image-4.*

4.5 Comparative Analysis

This section describes the analysis made using the existing methods, namely GHS_DBN, KNN, DBN, NN, SVM, AEDE, BBO, and the proposed Adaptive GHS-based Deep DCNN to the M-value and training data.

4.5.1 Analysis Based on M Value

The comparative analysis of the proposed Adaptive GHS-based Deep DCNN based on the M-value to the metrics, like accuracy, specificity, and sensitivity is explained in Fig. 5.Fig. 5 a) shows the analysis based on the M value to the accuracy. When the value of M is 20, the accuracy obtained by the existing methods, like DBN, SVM, BBO, GHS-DBN, KNN, NN, and AEDE is 0.64, 0.59, 0.68, 0.8, 0.59, 0.62, and 0.68, while the proposed Adaptive GHS-based deep CNN attained better accuracy with the value of 0.78, respectively. When the value of M is 10, the accuracy obtained by the proposed Adaptive GHS-based deep CNN is 0.86, when it is compared with the existing methods, such as DBN, SVM, BBO, GHS-DBN, KNN, NN, and AEDE, the percentage of improvement is reported as 13%, 39%, 6%, 2%, 6%, 39%, 16%, respectively. When the M value is 5, the accuracy obtained by the proposed Adaptive GHS-based deep CNN is 0.92, when it is compared with the existing methods, such as DBN, SVM, BBO, GHS-DBN, KNN, NN, and AEDE the percentage of improvement is reported as 12%, 56%, 5%, 2%, 11%, 100%, and 77%.

Fig. 5 b) depicts the analysis based on the M-value to the specificity. When the value of M is 20, the specificity obtained by the existing methods, like DBN, SVM, BBO, GHS-DBN, KNN, NN, and AEDE is 0.864, 0.6742, 0.8253, 0.8711, 0.8339, 0.7682, 0.8366, while the proposed Adaptive GHS-based deep CNN attained better specificity with the value of 0.8730, respectively. When the value of M is 10, the specificity obtained by the proposed Adaptive GHS-based deep CNN is 0.92, when it is compared with the existing methods, such as DBN, SVM, BBO, GHS-DBN, KNN, NN, and AEDE, the percentage of improvement is 7%, 36%, 5%, 1.3%, 6.5%, 24%, 76%, respectively. When the M value is 5, the specificity obtained by the proposed Adaptive GHS-based deep CNN is 0.95, when it is compared with the existing methods, such as DBN, SVM, BBO, GHS-DBN, KNN, NN, and AEDE, the percentage of improvement is reported as 4%, 40%, 5%, 1%, 7%, 41%, and 26%.

Fig. 5 c) shows the analysis based on the M value to the sensitivity. When the value of M is 20, the sensitivity obtained by the existing methods, like DBN, SVM, BBO, GHS-DBN, KNN, NN, and AEDE is 0.7460, 0.5071, 0.7093, 0.7556, 0.7373, 0.6524, and 0.6794, while the proposed Adaptive GHS-based deep CNN attained better sensitivity with the value of 0.7556, respectively. When the value of M is 10, the sensitivity obtained by the proposed Adaptive GHS-based deep CNN is 0.84, when it is compared with the existing methods, such as DBN, SVM, BBO, GHS-DBN, KNN, NN, and AEDE, the percentage of improvement is reported as 17%, 67%, 5%, 2%, 5.5%, 43%, and 17%, respectively. When the M value is 5, the sensitivity obtained by the proposed Adaptive GHS-based deep CNN is 0.92, when it is compared with the existing methods, such as DBN, SVM, BBO, GHS-DBN, KNN, NN, and AEDE, the percentage of improvement is reported as 10%, 81%, 4%, 2%, 11%, 99%, and 78%.

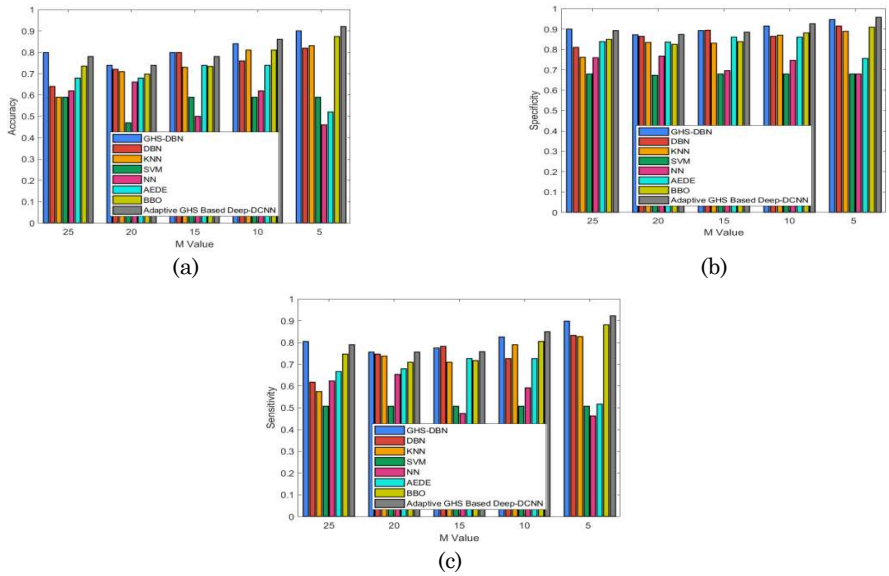

(a) (b) (c)

Fig. 5. Analysis using M value, a) Accuracy, b) Specificity, c) Sensitivity

4.5.2 Analysis Based on Training Data

The comparative analysis of the proposed Adaptive GHS-based Deep DCNN based on the training data to the metrics, namely accuracy, specificity, and sensitivity is depicted in Fig. 6.Fig. 6 a) shows the analysis based on the training data to the accuracy. When the training data is 60%, the accuracy obtained by the existing methods, like DBN, SVM, BBO, GHS-DBN, KNN, NN, and AEDE, is 0.857, 0.356, 0.700, 0.905, 0.744, 0.448, and 0.700, while the proposed Adaptive GHS-based deep CNN attained better accuracy with the value of 0.830, respectively. When the training data is 80%, the accuracy obtained by the existing methods, like DBN, SVM, BBO, GHS-DBN, KNN, NN, and AEDE is 0.838, 0.356, 0.840, 0.929, 0.860, 0.511, and 0.720, while the proposed Adaptive GHS-based deep CNN attained better accuracy with the value of 0.950, respectively. When the training data is 90%, the accuracy obtained by the existing methods, like DBN, SVM, BBO, GHS-DBN, KNN, NN, and AEDE is 0.789, 0.356, 0.900, 0.954, 0.900, 0.346, and 0.760, while the proposed Adaptive GHS-based deep CNN attained better accuracy with the value of 0.970, respectively.

Fig. 6 b) depicts the analysis based on the training data to the specificity. When the training data is 50%, the specificity obtained by the existing methods, like DBN, SVM, BBO, GHS-DBN, KNN, NN, and AEDE is 0.9195, 0.6804, 0.8083, 0.9540, 0.8411, 0.6548, and 0.8738, while the proposed Adaptive GHS-based deep CNN attained better specificity with the value of 0.9357, respectively. When the training data is 80%, the specificity obtained by the proposed Adaptive GHS-based deep CNN is 0.98, when it is compared with the existing methods, such as DBN, SVM, BBO, GHS-DBN, KNN, NN, and AEDE, the percentage of improvement is reported as 7%, 44%, 7%, 2%, 6%, 31%, and 15%, respectively. When the training data is 90%, the specificity obtained by the proposed Adaptive GHS-based deep CNN is 0.99, when it is compared with the existing methods, such as DBN, SVM, BBO, GHS-DBN, KNN, NN, and AEDE, the percentage of improvement is reported as 11%, 46%, 4%, 1%, 4%, 47%, and 13%.

Fig. 6 c) shows the analysis based on the training data to the sensitivity. When the training data is 50%, the sensitivity obtained by the existing methods, like DBN, SVM, BBO, GHS-DBN, KNN, NN, and AEDE is 1, 1, 0.6190, 1, 0.7619, 0.8, and 0.7429, while the proposed Adaptive GHS-based deep CNN attained better sensitivity with the value of 0.8698, respectively. When the training data is 80%, the sensitivity obtained by the existing methods, like DBN, SVM, BBO, GHS-DBN, KNN, NN, and AEDE is 1, 1, 0.837, 1, 0.8667, 0.571, and 0.721, while the proposed Adaptive GHS-based deep CNN attained better sensitivity with the value of 0.970, respectively.

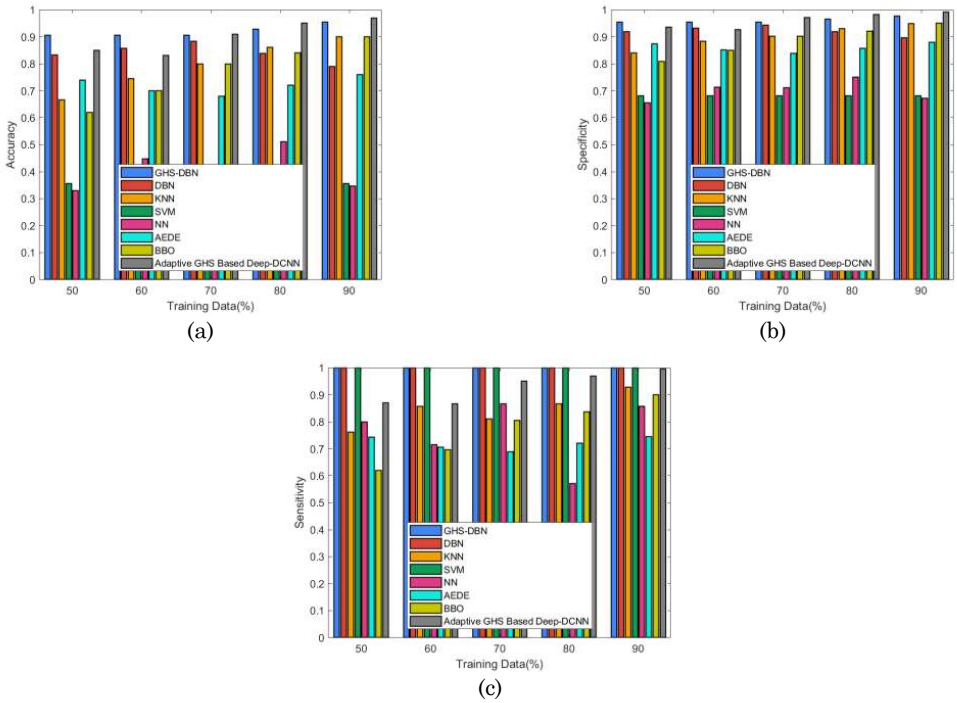

Fig. 6. Analysis using training data, a) Accuracy, b) Specificity, c) Sensitivity

4.5.3 ROC Analysis

Fig. 7 shows the ROC analysis graph for osteoporosis classification. When the FPR value is 0.5, the TPR attained by the existing methods, like DBN, SVM, BBO, GHS-DBN, KNN, NN, and AEDE is 0.50, 0.44, 0.67, 0.78, 0.31, 0.33, and 0.69, while the proposed Adaptive GHS-based deep CNN obtained the TPR as

0.9, respectively. Hence, the proposed Adaptive GHS-based deep CNN attained a higher TPR value for the minimal error.

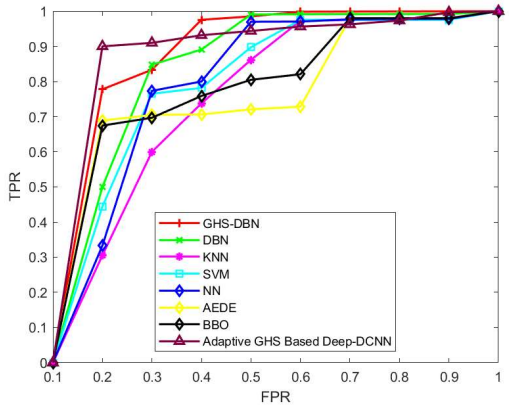

Fig. 7. ROC analysis

4.6 Comparative Discussion

This section describes the comparative discussion of the proposed Adaptive GHS-based deep CNN for the osteoporosis classification. The maximum values attained by the existing methods, like DBN, SVM, BBO, GHS-DBN, KNN, NN, and AEDE for the metrics accuracy to the M value is 0.82, 0.59, 0.873, 0.9, 0.83, 0.46, and 0.52, whereas the proposed Adaptive GHS-based deep CNN attained the maximum value as 0.92, respectively. Moreover, the maximum values attained by the existing methods, like DBN, SVM, BBO, GHS-DBN, KNN, NN, and AEDE for the metrics sensitivity to the training data is 1, 1, 0.9, 1, 0.928, 0.857, and 0.7444.

Table 2. *Comparative discussion*

Metrics		GHS-DBN	DBN	KNN	SVM	NN	AEDE	BBO	Adaptive GHS-based deep CNN
Accuracy	*M value*	0.9	0.82	0.83	0.59	0.46	0.52	0.873	0.92
	Training data (%)	0.953	0.788	0.9	0.3555	0.346	0.76	0.9	0.97
Specificity	*M value*	0.9467	0.9146	0.8892	0.6801	0.6798	0.7562	0.9094	0.9582
	Training data (%)	0.9770	0.896	0.9487	0.6804	0.6721	0.8803	0.9507	0.9910
Sensitivity	*M value*	0.8984	0.8333	0.8262	0.5071	0.4635	0.5175	0.8819	0.9222
	Training data (%)	1	1	0.9285	1	0.857	0.7444	0.9	0.995

5. Conclusion

Osteoporosis affects the bones and leads to bone fragility through minimizing the bone density. The fracture in the bone causes severe backache, height loss, and bone deformities, which significantly affect the vertebrae. The Adaptive Harmony Search-based Deep Convolutional Neural Network is proposed in this research to achieve the osteoporosis classification in the X-ray images. At first, the input X-ray images are pre-processed and the interesting regions are extracted. The extracted regions are further processed by the segmentation phase, which uses the mean shift clustering technique for extracting the femur boundaries. The femur boundaries are extracted using the femur bone geometric estimation phase, where the template search method is used to mark the femur points automatically. The features, like medical-level features, image-level features, and pixel-level features are effectively extracted. Finally, the osteoporosis classification is performed using the Deep Convolutional Neural Network, which is trained by the proposed Adaptive Gradient Harmony Search optimization. The proposed Adaptive Gradient Harmony Search-based Deep Convolutional Neural Network classifier attained better performance for the metrics, namely accuracy, specificity, and sensitivity with the values of 0.97, 0.99, and 0.99, respectively.

Compliance with Ethical Standards

Conflicts of interest: Authors declared that they have no conflict of interest.

Human participants: The conducted research follows the ethical standards and the authors ensured that they have not conducted any studies with human participants or animals.

References

[1] Areeckal A.S. and Kocher M, "Current and emerging diagnostic imaging-based techniques for assessment of osteoporosis and fracture risk", IEEE Reviews in Biomedical Engineering, vol. 12, pp.254-268, 2019.

[2] Devikanniga D. and Raj R.J.S., "Classification of osteoporosis by artificial neural network based on monarch butterfly optimization algorithm", Healthcare Technology Letters, vol. 5, no. 2, pp.70-75, 2018.

[3] Hussain D. and Han S.M., "Computer-Aided Osteoporosis Detection from DXA Imaging",Computer Methods and Programs in Biomedicine, 2019.

[4] Aouache M., Hussain A., Zulkifley M.A., Zaki D.W.M.W., Husain H., and Hamid H.B.A., "Anterior osteoporosis classification in cervical vertebrae using fuzzy decision tree", Multimedia Tools and Applications, vol. 77, no. 3, pp.4011-4045, 2018.

[5] Gazzotti M.R., Roco C.M., Pradella C.O., Nascimento O.A., Porto E.F., Adas M., Lazaretti-Castro M. and Jardim J.R., "Frequency of Osteoporosis and Vertebral Fractures in Chronic Obstructive Pulmonary Disease (COPD) Patients", Archivos de bronconeumologia. 2018.

[6] Aslan M.S, Shalaby A., and Farag A.A.,"Vertebral body segmentation using a probabilistic and universal shape model",IET Computer Vision, vol. 9, no. 2, pp.234-250, 2014.

[7] Kavitha M.S., Ganesh Kumar P., Park S.Y., Huh K.H., Heo M.S., Kurita T., Asano A., An, S.Y. and Chien, S.I., "Automatic detection of osteoporosis based on hybrid genetic swarm fuzzy classifier approach", Dentomaxillofacial Radiology, vol. 45, no. 7, pp.20160076, 2016.

[8] Deleskog L., Laursen N.Ø., Nielsen B.R., and Schwarz P, "Vertebral fracture assessment by DXA is inferior to X-ray in clinical severe osteoporosis", Osteoporosis International, vol. 27, no. 7, pp.2317-2326, 2016.

[9] Bazzocchi A., Spinnato P., Fuzzi F., Diano D., Morselli-Labate A.M., Sassi C., Salizzoni E., Battista, G., and Guglielmi G., "Vertebral fracture assessment by new dual-energy X-ray absorptiometry", Bone, vol. 50, no. 4, pp.836-841, 2012.

[10] Bliuc D, Nguyen T.V., and Eisman J.A., "Risk of subsequent fracture after low-trauma fracture in men and women", Jama, vol. 297, no. 4, pp.387-394, 2007.

[11] Johnell O. and Kanis J., "Epidemiology of osteoporotic fractures", Osteoporosis international, vol. 16, no. 2, pp.S3-S7, 2005.

[12] Adams J.E., "Quantitative computed tomography", European Journal of Radiology, vol. 71, no. 3, pp.415-424, 2009.

[13] Harvey N.C., McCloskey E.V., Mitchell P.J., Dawson-Hughes B., Pierroz D.D., Reginster J.Y., Rizzoli R., Cooper C., and Kanis J.A., "Mind the (treatment) gap: a global perspective on current and future strategies for prevention of fragility fractures", Osteoporosis International, vol. 28, no. 5, pp.1507-1529, 2017.

[14] Cabral H.W.S., Andolphi B.F.G., Ferreira B.V.C., Alves D.C.F., Morelato R.L., Chambo Filho A., and Borges L.S., "The use of biomarkers in clinical osteoporosis", Revista da Associação Médica Brasileira, vol. 62, no. 4, pp.368-376, 2016.

[15] Looker A.C., Bauer D.C., Chesnut Iii C.H., Gundberg C.M., Hochberg M.C., Klee, G., Kleerekoper M., Watts, N.B., and Bell N.H., "Clinical use of biochemical markers of bone remodeling: current status and future directions", Osteoporosis International, vol. 11, no. 6, pp.467-480, 2000.

[16] Ordóñez C., Matías J.M., de Cos Juez J.F., and García P.J., "Machine learning techniques applied to the determination of osteoporosis incidence in post-menopausal women", Mathematical and Computer Modelling, vol. 50, no. 5, pp.673-679, 2009.

[17] Xu Y., Li D., Chen, Q., and Fan Y., "Full supervised learning for osteoporosis diagnosis using micro-CT images", Microscopy research and technique, vol. 76, no. 4, pp.333-341, 2013.

[18] Tafraouti A., El Hassouni M., Toumi H., Lespessailles E, and Jennane R., "Osteoporosis diagnosis using fractal analysis and support vector machine", IEEE Tenth International Conference on Signal-Image Technology and Internet-Based Systems, pp. 73-77, November 2014.

[19] Chang H.W., Chiu Y.H., Kao H.Y., Yang C.H., and Ho W.H., "Comparison of classification algorithms with wrapper-based feature selection for predicting osteoporosis outcome based on genetic factors in a Taiwanese women population", International journal of endocrinology, 2013.

[20] Melton Iii L.J., Atkinson E.J., Cooper C., O Fallon, W.M., and Riggs B.L., "Vertebral fractures predict subsequent fractures", Osteoporosis International, vol. 10, no. 3, pp.214-221, 1999.

[21] Ross P.D., Genant H.K., Davis J.W., Miller P.D., and Wasnich R.D., "Predicting vertebral fracture incidence from prevalent fractures and bone density among non-black", osteoporotic women, Osteoporosis International, vol. 3, no. 3, pp.120-126, 1993.

[22] Kanis J.A., "Diagnosis of osteoporosis and assessment of fracture risk", The Lancet, vol. 359, no. 9321, pp.1929-1936, 2002.

[23] Dendere R., Potgieter J.H., Steiner S., Whiley S.P., and Douglas T.S., "Dual-energy x-ray absorptiometry for measurement of phalangeal bone mineral density on a slot-scanning digital radiography system", IEEE Transactions on Biomedical Engineering, vol. 62, no. 12, pp.2850-2859, 2015.
[24] Rawat W. and Wang Z., "Deep convolutional neural networks for image classification: A comprehensive review", Neural Computation, vol. 29, no. 9, pp.2352-2449, 2017.
[25] Prithwish Chakraborty, Gourab Ghosh Roy, Swagatam Das, Dhaval Jain, Ajith Abraham, "An Improved Harmony Search Algorithm with Differential Mutation Operator", Fundamenta Informaticae - Swarm Intelligence, Vol. 95, No. 4, pp. 401-426, December 2009.
[26] D. Comaniciu and P. Meer, "Mean shift: a robust approach toward feature space analysis," in IEEE Transactions on Pattern Analysis and Machine Intelligence, vol. 24, no. 5, pp. 603-619, May 2002.
[27] Vojt, B.J. "Deep neural networks and their implementation", Document number 159717, 2016.
[28] Deng, Z. Zhu, X. Cheng, D. Zong, M and Zhang, S. "Efficient kNN classification algorithm for big data. Neurocomputing", vol. 195, 143-148, 2016.
[29] Boser, B.E. Guyon, I.M. Vapnik, V.N., "A training algorithm for optimal margin classifiers", in proceedings of the fifth annual workshop on Computational learning theory COLT, Pittsburgh, Pennsylvania, USA, ACM Digital Library, pp. 144-152, 1992.
[30] Mirjalili, S. Mirjalili, S.M and Lewis, A. "Let a biogeography-based optimizer train your Multi-Layer Perceptron", Information Sciences. vol. 269, pp. 188-209, 2014.
[31] Demertzis K. and Iliadis L., "Adaptive elitist differential evolution extreme learning machines on big data: intelligent recognition of invasive species", In INNS Conference on Big Data, Springer, Cham, pp. 333-345, October 2016.
[32] Hwang, D.H., Bak, S.H., Ha, T.J., Kim, Y., Kim, W.J. and Choi, H.S., "Multi-View Computed Tomography Network for Osteoporosis Classification", *IEEE Access*, Vol. *11*, pp.22297-22306, 2023.
[33] Zhang, K., Lin, P., Pan, J., Xu, P., Qiu, X., Crookes, D., Hua, L. and Wang, L., "End to End Multitask Joint Learning Model for Osteoporosis Classification in CT Images", Computational Intelligence and Neuroscience, 2023.
[34] Alqahtani, F.F. and Bromiley, P.A., "Accuracy of Using a New Semi-Automated Software Package to Diagnose Osteoporotic Vertebral Fractures in Adults", Electronics, Vol. 12(4), p.847, 2023.
[35] Albuquerque, G.D.A., de Carvalho, D.D., Cruz, A.S., Santos, J.P.Q., Machado, G.M., Gendriz, I.S., Fernandes, F.R., Barbalho, I.M., Santos, M.M., Teixeira, C.A. and Henriques, J.M., "A Machine Learning based approach to osteoporosis classification: a correlational and comparative analysis between Osseus and DXA exams", 2023.
[36] Hsu, P.C., Luzhbin, D., Shih, T.Y. and Wu, J., "Diagnosis of Osteoporosis by Quantifying Volumetric Bone Mineral Density of Lumbar Vertebrae Using Abdominal CT Images and Two-Compartment Model", In Healthcare (Vol. 11, No. 4, p. 556), MDPI. 2023, February.
[37] Al-Bogami, M.M., Akanle, O.A., Aldawood, S., Alkhorayef, M., Sulieman, A., Jawad, A.S. and Mageed, R.A., "Comparison of bone mineral density changes between male and female osteoporosis patients using dual-energy X-ray absorptiometry scan", Applied Radiation and Isotopes, Vol. 194, pp.110624, 2023.
[38] Wani, I.M. and Arora, S., "Osteoporosis diagnosis in knee X-rays by transfer learning based on convolution neural network", Multimedia Tools and Applications, pp.1-25, 2022.
[39] Mohammed, A.Z. and George, L.E., 'Osteoporosis detection using convolutional neural network based on dual-energy X-ray absorptiometry images", Indonesia. J. Electr. Eng. Comput. Sci, Vol. 29(1), pp.315, 2022.